Equilibrium studies of a poloidal divertor pinch with a reversed toroidal field

J. S. Sarff, J. C. Sprott, and L. Turner[a)]
Department of Physics, University of Wisconsin, Madison, Wisconsin 53706

(Received 13 November 1986; accepted 26 March 1987)

An analytic solution for the force-free magnetic field, $\nabla\times\mathbf{B}=\lambda\,\mathbf{B}$, in the poloidal divertor configuration of the Tokapole II device [Nucl. Fusion **19**, 1509 (1979)] is presented. Experiments conducted on Tokapole II which provide equilibrium magnetic field profile measurements using a magnetic probe are then described. Observations include a non-constant-λ profile and a large diamagnetic current near the magnetic separatrix.

I. INTRODUCTION

The reversed-field pinch (RFP)[1,2] is an axisymmetric toroidal plasma confinement system. Many RFP experiments[3] have operated since 1965 when toroidal field reversal was correlated with increased stability and better confinement on the ZETA experiment.[4] The long-lived plasma equilibria observed in present machines, violating naive arguments[5,6] that predict their decay via resistive diffusion, have generated great interest within the fusion community. The use of a minimum-energy principle that appears to account for these reversed-field equilibria was suggested by Taylor.[7] Such variational principles had been introduced into astrophysics earlier, as well as into fusion physics.[8] In Taylor's model, these equilibria are described by the zero-beta magnetohydrodynamic equilibrium equation,

$$\nabla\times\mathbf{B}=\lambda\,\mathbf{B},\quad \lambda=\text{const.}$$

The one-dimensional axisymmetric solutions of this equation in a long cylinder are well known to be Bessel functions and are called the Bessel function model (BFM).

The success of the constant-λ model in predicting RFP equilibria leads to the consideration of its applicability to other geometries. It appears that the salient features of the equilibria in the spheromak[9,10] and multipinch,[11] a noncircular RFP with a magnetic well, are described by the constant-λ model. The geometry considered here is that of the Tokapole II device,[12] normally operated as a four-node poloidal divertor tokamak which can be also operated with a programmed-reversed toroidal field.

This paper presents the Taylor equilibria of this divertor configuration and the actual equilibria obtained from experiments performed on Tokapole II.

The sustainment of the equilibria and the general improvement in plasma quality associated with the reversed toroidal field are attributes of the RFP that are attractive for fusion purposes. We are ultimately concerned with the effect of the divertor geometry on sustainment and plasma quality.

Using existing techniques, it is straightforward to obtain two-dimensional analytic solutions of $\nabla\times\mathbf{B}=\lambda\,\mathbf{B}$ in the Tokapole II geometry. However, evidence from the tokamak operation of Tokapole II shows the plasma current is largely confined within the magnetic separatrix (see Fig. 3 for a description of the nomenclature used for Tokapole II flux regions). The relatively current-free, high-field-strength regions of common and private flux must have lower λ values than that of the large current density, low-field-strength region within the separatrix. The constant-λ solutions are therefore unlikely to be an accurate description of the magnetic field topology in Tokapole II.

Although the constant-λ model predicts the stark feature of a reversed toroidal magnetic field near the edge of the RFP plasma, a constant-λ profile provides too simplistic a description of the magnetic field in the RFP. The modified Bessel function model (MBFM), which assumes λ is constant over the interior of the plasma but decreasing linearly to zero at the edge, provides better agreement with the experiments.[13] An Ohmic force-free paramagnetic plasma naturally exhibits a non-constant-λ profile.[6] The decrease in λ results from a decrease in the parallel electric field ($\mathbf{E}\cdot\mathbf{B}/B$) as well as the observed increase in plasma resistivity in the outer region of the plasma. These same effects occur in Tokapole II as well, but the conducting rings, which generate a magnetic field nearly orthogonal to the applied electric field, force a decrease in the parallel electric field far from the conducting wall.

The constant-λ equilibria of the RFP are completely specified by two parameters, whereas the corresponding equilibria in Tokapole II require the additional specification of the values of the ring currents. Because of the complication created by the presence of the rings and the expectation that λ is not constant, equilibrium magnetic field profiles were obtained along the midplane of Tokapole II using a movable magnetic probe.

II. ANALYTIC SOLUTION OF $\nabla\times\mathbf{B}=\lambda\mathbf{B}$ IN TOKAPOLE II GEOMETRY

For simplicity, we ignore toroidal effects and model Tokapole II as a long straight tube. Our solution will be obtained for an arbitrary rectangular cross-sectional tube although we will evaluate it here only for the special case of a square cross section to model Tokapole II.

Choosing the z direction to be along the tube, we wish to solve $\nabla\times\mathbf{B}(x,y)=\lambda\,\mathbf{B}(x,y)$, where $\mathbf{B}$ is subject to the boundary condition that its normal component vanishes at the surface of the perfectly conducting rectangular boundary. The boundary is assumed to stretch from 0 to a along the x axis and from 0 to b along the y axis. Setting

$$\mathbf{B}=\lambda\nabla\times\phi\hat{z}+\nabla\times(\nabla\times\phi\hat{z})=\lambda\nabla\phi\times\hat{z}-\nabla^2\phi\hat{z},\qquad(1)$$

where ϕ satisfies

[a)] Permanent address: Los Alamos National Laboratory, University of California, Los Alamos, New Mexico 87545.

 0031-9171/87/072155-08$01.90

$$(\nabla^2 + \lambda^2)\phi(x,y) = S(x,y), \tag{2}$$

and where

$$\frac{\partial \phi}{\partial z} = 0,$$

we reduce our problem to the determination of a scalar potential $\phi(x,y)$. The boundary condition on $\mathbf{B}$ requires that ϕ be a constant, say ϕ_0, on the boundary. Note that Eq. (1) implies that

$$B_x = \lambda \frac{\partial \phi}{\partial y}, \quad B_y = -\lambda \frac{\partial \phi}{\partial x}, \quad B_z = \lambda^2 \phi.$$

Here $S(x,y)$ is a source function to be determined by the positions and values of the filamentary current sources which are idealizations of Tokapole II's internal conducting rings.

If we make the transformation from ϕ to χ,

$$\chi(x,y) = \phi(x,y) - \phi_0, \tag{3}$$

we find that χ satisfies the inhomogeneous Helmholtz equation

$$(\nabla^2 + \lambda^2)\chi(x,y) = -\lambda^2 \phi_0 + S(x,y)$$

subject to the homogeneous boundary condition, $\chi|_{b'd'y} = 0$.

Therefore if we know the Green's function $G(\mathbf{r},\mathbf{r}')$ that satisfies

$$(\nabla^2 + \lambda^2)G(\mathbf{r},\mathbf{r}') = \delta^{(2)}(\mathbf{r} - \mathbf{r}') \tag{4}$$

with homogeneous Dirichlet boundary conditions, then

$$\chi(x,y) = \int_0^b dy' \int_0^a dx' [-\lambda^2 \phi_0 + S(x',y')] G(x,y;x',y'). \tag{5}$$

The Green's function can be represented as

$$G(\mathbf{r},\mathbf{r}') = \sum_{n=1}^{\infty} G_n^x(x,x') G_n^y(y,y'), \tag{6}$$

where

$$G_n^x(x,x') = \sin k_n x' \sin k_n x, \tag{7}$$

where, for $\lambda^2 \geqslant k_n^2$,

$$G_n^y(y,y') = C_n \sin \alpha_{-n} y_< [\sin \alpha_{-n} y_> \cos \alpha_{-n} b - \cos \alpha_{-n} y_> \sin \alpha_{-n} b] \tag{8a}$$

and, for $\lambda^2 < k_n^2$,

$$G_n^y(y,y') = C_n \sinh \alpha_{+n} y_< [\sinh \alpha_{+n} y_> \cosh \alpha_{+n} b - \cosh \alpha_{+n} y_> \sinh \alpha_{+n} b]. \tag{8b}$$

We are using the definitions

$$k_n = n\pi/a, \quad \alpha_{\pm n} = [\pm (k_n^2 - \lambda^2)]^{1/2},$$

and the convention that $y_>$ ($y_<$) represents the greater (lesser) of y and y'. The values of the C_n's are determined by inserting Eqs. (6) and (7) into Eq. (4), which yields

$$\frac{\partial^2 G_n^y(y,y')}{\partial y^2} + (\lambda^2 - k_n^2) G_n^y(y,y') = \frac{2}{a} \delta(y - y').$$

If we integrate this result over the interval $y = y' - \epsilon$ to $y = y' + \epsilon$ and then let $\epsilon \to 0$, we obtain

$$\lim_{\epsilon \to 0} \frac{\partial G_n^y}{\partial y}\bigg|_{y = y' - \epsilon}^{y = y' + \epsilon} = \frac{2}{a}. \tag{9}$$

By inserting Eqs. (8) into Eq. (9), we obtain the values of the C_n's:

$$C_n = \frac{2}{a\alpha_{-n} \sin \alpha_{-n} b} \quad (\text{for } \lambda^2 \geqslant k_n^2), \tag{10a}$$

or

$$C_n = \frac{2}{a\alpha_{+n} \sinh \alpha_{+n} b} \quad (\text{for } \lambda^2 < k_n^2). \tag{10b}$$

From Eqs. (6)–(8) and (10), we derive the final result for $G(\mathbf{r},\mathbf{r}')$,

$$G(\mathbf{r},\mathbf{r}') = \frac{2}{a} \sum_{n \leqslant n^*} \frac{\sin k_n x \sin k_n x'}{\alpha_{-n} \sin \alpha_{-n} b} \times [\sin \alpha_{-n} y_< \sin \alpha_{-n} (y_> - b)] + \frac{2}{a} \sum_{n > n^*} \frac{\sin k_n x \sin k_n x'}{\alpha_{+n} \sinh \alpha_{+n} b} \times [\sinh \alpha_{+n} y_< \sinh \alpha_{+n} (y_> - b)] \tag{11}$$

in which n^* is the maximum value of n such that $\lambda^2 \geqslant k_n^2$. We shall use the notation $G_v(\mathbf{r},\mathbf{r}')$ to represent the Green's function for the vacuum case when $\lambda = 0$. One notes immediately that

$$G_v(\mathbf{r},\mathbf{r}') = \frac{2}{a} \sum_{n=1}^{\infty} \frac{\sin k_n x \sin k_n x'}{k_n \sinh k_n b} \times [\sinh k_n y_< \sinh k_n (y_> - b)]. \tag{12}$$

We next turn to the determination of the source function $S(x,y)$. We first note that a straight filament carrying current I along the z axis generates a magnetic field in the neighborhood of the filament given by

$$B_\theta(r) = \mu_0 I / 2\pi r.$$

From our scalar representation [Eq. (1)] of the magnetic field, we note that

$$B_\theta = \lambda \nabla \phi \times \hat{z} = -\lambda \frac{\partial \phi}{\partial r} = \frac{\mu_0 I}{2\pi r}$$

or, equivalently, that

$$\phi = (-\mu_0 I / 2\pi\lambda) \ln r. \tag{13}$$

Thus near $r = 0$, ϕ is determined by the Poisson equation,

$$\nabla^2 \phi = \frac{1}{r} \frac{\partial}{\partial r}\left(r \frac{\partial \phi}{\partial r}\right) = \frac{-\mu_0 I}{\lambda} \frac{\delta(r)}{2\pi r},$$

in which neighborhood the $\lambda^2 \phi$ term of the Helmholtz equation is negligible. Since this result must be invariant under translation, we immediately obtain the structure of the source function,

$$S(\mathbf{r}) = \frac{-\mu_0}{\lambda} \sum_{i=1}^{n} I_i \delta^{(2)}(\mathbf{r} - \mathbf{r}_i), \tag{14}$$

in which the sum is being taken over the case of n currents $\{I_i\}$ positioned at the n positions $\{\mathbf{r}_i = (x_i, y_i)\}$, $i = 1,\ldots,n$. Inserting Eqs. (11) and (14) into Eq. (5) and using the identity[9]

$$\frac{4}{\pi}\sum_{\substack{n=1\\ \text{odd}}}^{\infty}\frac{\sin k_n x}{n(\lambda^2-k_n^2)}=\frac{1}{\lambda^2}\left(\frac{\sin\lambda(x-a)-\sin\lambda x}{\sin\lambda a}+1\right),$$

we obtain

$$\chi(\mathbf{r})=-\phi_0\left(1+\frac{\sin\lambda(x-a)-\sin\lambda x}{\sin\lambda a}\right)-\lambda^2\phi_0\left[\frac{4}{\pi}\sum_{n,\text{odd}\le n^*}\frac{\sin k_n x}{n\alpha_{-n}^2}\left(\frac{\sin\alpha_{-n}(y-b)-\sin\alpha_{-n}y}{\sin\alpha_{-n}b}\right)\right.$$
$$\left.+\frac{4}{\pi}\sum_{n,\text{odd}>n^*}\frac{\sin k_n x}{n\alpha_{+n}^2}\left(\frac{\sinh\alpha_{+n}y-\sinh\alpha_{+n}(y-b)}{\sinh\alpha_{+n}b}\right)\right]-\frac{\mu_0}{\lambda}\sum_{j=1}^{n}I_j G(\mathbf{r},\mathbf{r}_j). \tag{15}$$

In order to improve convergence of the sum, we shall isolate the logarithmic singularities of the final sum of Eq. (15). We can perform this isolation by adding to and subtracting from Eq. (15) two representations of the solution of

$$\nabla^2\phi=\frac{-\mu_0}{\lambda}\sum_{j=1}^{n}I_j\delta^{(2)}(\mathbf{r}-\mathbf{r}_j) \tag{16}$$

within the aforementioned perfectly conducting rectangular boundary. Note that this "vacuum" equation is obtained from Eq. (2) by letting λ equal zero on the left-hand side of Eq. (2).

The first representation of the solution can be obtained by the method of images. We already know [see Eq. (13)] the solution in an unbounded domain for a single filament at $\mathbf{r}_j$ carrying the current I_j:

$$\phi_{v_j}=(\mu_0 I_j/2\pi\lambda)\ln|\mathbf{r}-\mathbf{r}_j|.$$

The solution for the case of n filaments located within the rectangularly bounded region can be obtained from Eq. (13) by the method of images. One merely imagines a lattice of suitably arrayed positive and negative image currents and, thereby, obtains the representation

$$\phi_v^{(1)}(\mathbf{r})=\frac{-\mu_0}{4\pi\lambda}\sum_{j=1}^{n}I_j$$
$$\times\sum_{m,l=-\infty}^{+\infty}\ln\left(\frac{\{[x+(2al-x_j)]^2+[y+(2bm-y_j)]^2\}\{[x+(2al+x_j)]^2+[y+(2bm+y_j)]^2\}}{\{[x+(2al-x_j)]^2+[y+(2bm+y_j)]^2\}\{[x+(2al+x_j)]^2+[y+(2bm-y_j)]^2\}}\right).$$

To produce the second representation of the solution of Eq. (16), we express the solution in terms of the vacuum Green's function, Eq. (12):

$$\phi_v^{(2)}(\mathbf{r})=\frac{-\mu_0}{\lambda}\sum_{j=1}^{n}I_j\int G_v(\mathbf{r},\mathbf{r}')\delta^{(2)}(\mathbf{r}'-\mathbf{r}_j)d\mathbf{r}'.$$

This yields

$$\phi_v^{(2)}(\mathbf{r})=\frac{-2\mu_0}{\lambda a}\sum_{j=1}^{n}I_j\sum_{m=1}^{\infty}\frac{\sin k_m x\sin k_m x_j}{k_m\sinh k_m b}[\sinh k_m y_{<j}\sinh k_m(y_{>j}-b)],$$

where $y_{>j}(y_{<j})$ is the greater (lesser) of y and y_j. Replacing the final term of Eq. (15) with

$$\left(\frac{-\mu_0}{\lambda}\sum_{j=1}^{n}I_j G(\mathbf{r},\mathbf{r}_j)-\phi_v^{(2)}(\mathbf{r})\right)+\phi_v^{(1)}(\mathbf{r})$$

and using Eq. (3), we attain our final result for ϕ:

$$\phi(\mathbf{r})=-\phi_0\left(\frac{\sin\lambda(x-a)-\sin\lambda x}{\sin\lambda a}\right)$$
$$-\frac{4\lambda^2\phi_0}{\pi}\left[\sum_{n,\text{odd}\le n^*}\frac{\sin k_n x}{n\alpha_{-n}^2}\left(\frac{\sin\alpha_{-n}(y-b)-\sin\alpha_{-n}y}{\sin\alpha_{-n}b}\right)+\sum_{n,\text{odd}>n^*}\frac{\sin k_n x}{n\alpha_{+n}^2}\left(\frac{\sinh\alpha_{+n}y-\sinh\alpha_{+n}(y-b)}{\sinh\alpha_{+n}b}\right)\right]$$
$$-\frac{2\mu_0}{\lambda a}\sum_{j=1}^{n}I_j\left[\sum_{n\le n^*}\sin k_n x\sin k_n x_j\left(\frac{\sin\alpha_{-n}y_{<j}\sin\alpha_{-n}(y_{>j}-b)}{\alpha_{-n}\sin\alpha_{-n}b}-\frac{\sinh k_n y_{<j}\sinh k_n(y_{>j}-b)}{k_n\sinh k_n b}\right)\right.$$
$$\left.+\sum_{n>n^*}\sin k_n x\sin k_n x_j\left(\frac{\sinh\alpha_{+n}y_{<j}\sinh\alpha_{+n}(y_{>j}-b)}{\alpha_{+n}\sinh\alpha_{+n}b}-\frac{\sinh k_n y_{<j}\sinh k_n(y_{>j}-b)}{k_n\sinh k_n b}\right)\right]-\frac{\mu_0}{4\pi\lambda}\sum_{j=1}^{n}I_j$$
$$\times\sum_{m,l=-\infty}^{+\infty}\ln\left(\frac{\{[x+(2al-x_j)]^2+[y+(2bm-y_j)]^2\}\{[x+(2al+x_j)]^2+[y+(2bm+y_j)]^2\}}{\{[x+(2al-x_j)]^2+[y+(2bm+y_j)]^2\}\{[x+(2al+x_j)]^2+[y+(2bm-y_j)]^2\}}\right). \tag{17}$$

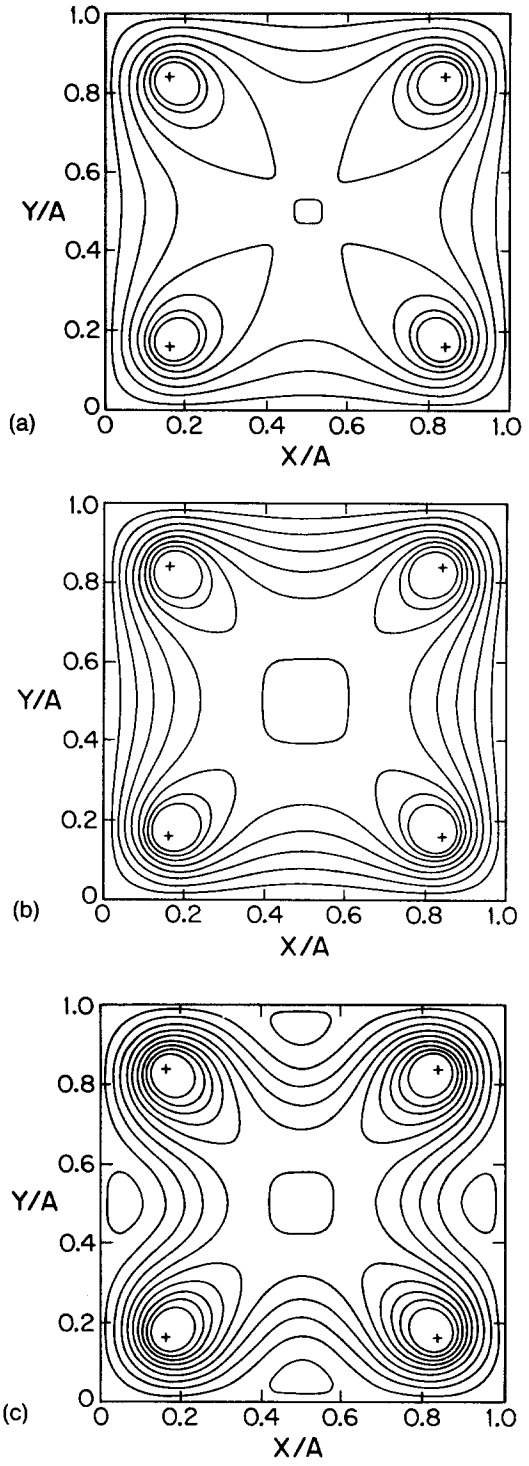

FIG. 1. Contours of B_z in a square with four filaments, each carrying 75 kA positioned at $(0.17a, 0.17a)$, $(0.17a, 0.83a)$, $(0.83a, 0.17a)$, and $(0.83a, 0.83a)$: (a) $a\lambda = 0.5$, $B_{z\,\text{boundary}} = 845$ G, $I_p = 17$ kA; (b) $a\lambda = 3.0$, $B_{z\,\text{boundary}} = -385$ G, $I_p = 62$ kA; and (c) $a\lambda = 10.0$, $B_{z\,\text{boundary}} = -3272$ G, $I_p = -166$ kA.

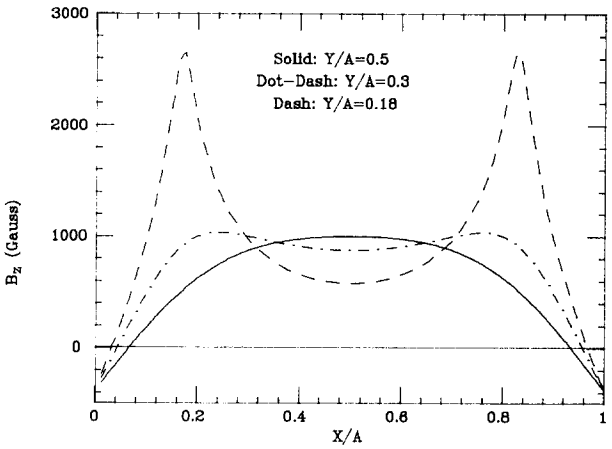

FIG. 2. Profiles of B_z for $a\lambda = 3.0$: The solid curve is $y/a = 0.5$, the dashed curve is $y/a = 0.18$, and the dot–dashed curve is $y/a = 0.3$.

We shall use our solution, Eq. (17), to describe flux contours and B_z profiles for the specific case of a square boundary with four current-bearing filaments placed near the corners along the diagonals of the square, i.e., Tokapole II's geometry. The contours denote equal increments of ϕ, that is, of B_z. The local tangent vectors to these contours are parallel (or antiparallel) to the local direction of $B_z\hat{x} + B_y\hat{y}$, where $\hat{x}$ and $\hat{y}$ are the unit vectors pointing, respectively, in the positive x and y directions.

In Fig. 1 we display these contours as a function of $a\lambda$ with the value of B_z at the center of the square and the values of the current filaments held fixed. In this sequence of figures, one observes the formation of a magnetic separatrix whose x points move increasingly close to the filaments. We also observe the formation of islands located between the current-bearing filaments when λ is increased. This behavior is associated with the lack of symmetry about the z axis as a result of the square boundary and the existence of the current filaments.

In Fig. 2 we display B_z profiles for the $a\lambda = 3.0$ case along three chords of constant y/a: on the symmetry line, near the filaments, and an intermediate chord. Note that the profiles are nearly flat in the central region with the strong gradients occurring near the edge. Also note the extremely large axial current density ($J_z = \lambda B_z$) near the filaments resulting from the force-free nature of the equilibria; this is the type of current unlikely to be realized in a real device.

We wish to note finally that by taking a line integral of **B** around the square boundary, we can determine the plasma current. The values of the plasma currents for the cases described in Fig. 1 above are listed in the associated captions. We also list the (constant) value of B_z at the boundary having fixed the value of B_z at 1000 G at the center of the square. Each filament bears 75 kA and is positioned along the diagonal a distance $0.24a$ from a corner. The length of the square's edge, a, is fixed at 44 cm. These numbers, which are similar to those in the experiment, will allow direct comparison of profiles.

III. EXPERIMENTAL DETERMINATION OF EQUILIBRIUM PROFILES

As was briefly discussed in the Introduction, Tokapole II is a small device (44 cm square cross section; major radius of 50 cm) designed to operate as a poloidal divertor tokamak. The magnetic divertor is produced by inductively driving four internal conducting rings in parallel with the dis-

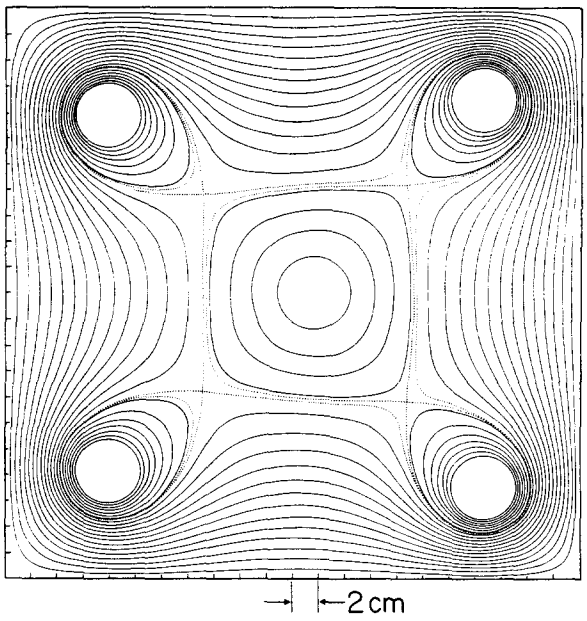

FIG. 3. A typical flux plot for the poloidal divertor tokamak configuration in Tokapole II. The separatrices are shown as dotted lines, and the surfaces that link all five currents are called common flux surfaces while the surfaces linking just one ring are called private flux surfaces.

charge. A typical flux plot is shown in Fig. 3. The central region is set up as a tokamak with the majority of the plasma current confined within the magnetic separatrix.

Attempting to form a reversed toroidal field in this same divertor configuration, a current was applied in the toroidal field windings which was forced to reverse direction after the initiation of the plasma current. Similar programming is used routinely on present day RFP experiments.[1] Typical waveforms of the electrical parameters are shown in Fig. 4.

To obtain magnetic field profiles, a single coil magnetic probe was inserted and moved radially along the midplane from the wall to the geometric axis. Several discharges were averaged to produce a data point at various radii thus constructing a profile. A decrease in the plasma current occurred with the probe inserted, but this was generally small ($\sim$10%–20%), and the data obtained are believed to be

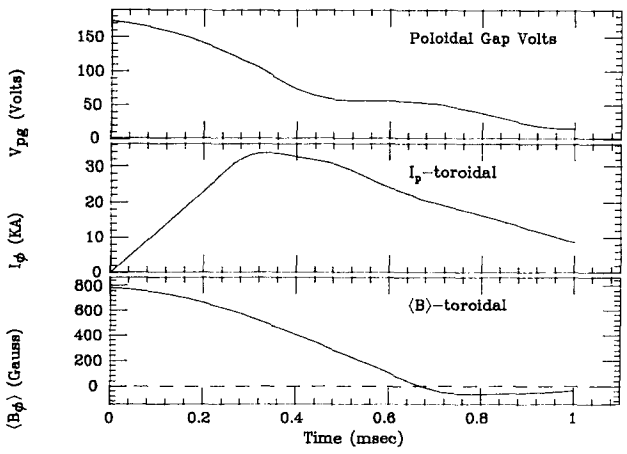

FIG. 4. Representative waveforms of the programmed-reversed mode of operation. The toroidal field is the average toroidal field defined as flux/a^2, where a = 44 cm for Tokapole II.

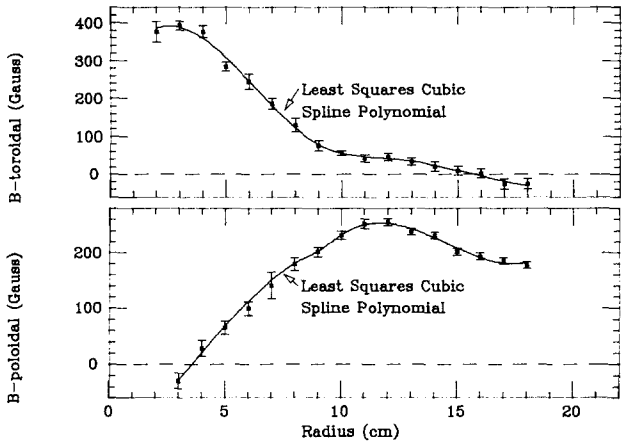

FIG. 5. Typical toroidal and poloidal (plasma component) field profile data with the fitted least-squares polynomials superimposed. The data shown were taken at 680 μsec.

representative of the unperturbed plasma. The use of probes in this fashion is not a new technique; recent studies using magnetic probes have been made on RFP's to obtain the equilibrium structure and to study fluctuations.[14,15]

The reversal point moved inward from the wall and disappeared at the center in a time period of $\sim$50–100 μsec, leaving the toroidal field reversed everywhere thereafter. Coincident with reversal occurred a "quiet" period of reduced fluctuations both in the edge magnetic field and plasma density (determined with a Langmuir probe biased to collect ion saturation current); the reduction in amplitude was at least a factor of 5. The fields and currents were decaying so that sustained reversed-field plasmas were not obtained. Nevertheless the decay was probably slow enough that the plasma relaxed through successive equilibria since a typical poloidal Alfvén time for these plasmas is a few microseconds. This time period, when there was a reversal point in the plasma, was examined in detail.

Least-square polynomial fits to the magnetic field profile data were used to obtain the current density profiles and λ profiles through the relations

$$\nabla\times\mathbf{B}=\mu_0\mathbf{J},\quad \lambda_{\parallel}=\frac{J_{\parallel}}{B}=\frac{\mathbf{J}\cdot\mathbf{B}}{B^2},\quad \lambda_{\perp}=\frac{J_{\perp}}{B}=\frac{|\mathbf{J}\times\mathbf{B}|}{B^2}.$$

To perform these calculations, toroidal axisymmetry has been assumed. For the calculation of the toroidal current density, the additional assumptions of a uniform horizontal equilibrium shift of the flux surfaces within the separatrix and that the poloidal magnetic field generated by the toroidal plasma current is nearly cylindrically symmetric were made. The latter assumption is the most severe, leading to an overestimate of the toroidal current density in the region near the separatrix of at most $\sim$8% of the axis (peak) value; no attempt was made to correct for this error. Examples of typical data for the toroidal field and the plasma generated poloidal field profiles with fitted polynomials are shown in Fig. 5. Figure 6 shows a time step sequence of the polynomial fits demonstrating the field decay, and Figs. 7 and 8 show profiles of the derived quantities at an intermediate time. The error bars shown represent the statistical accuracy of the data.

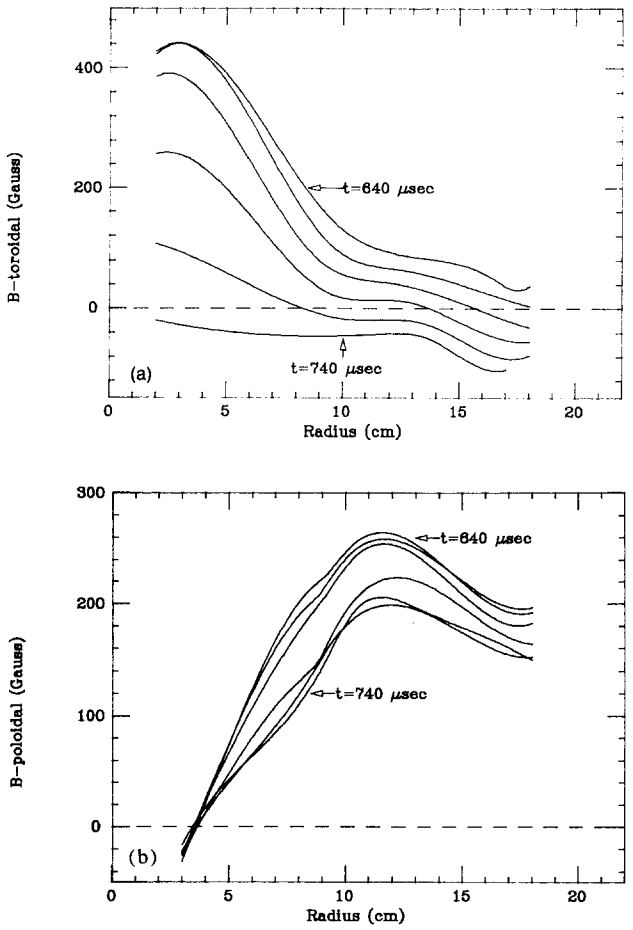

FIG. 6. Radial profiles of the (a) toroidal field and (b) poloidal field as a result of plasma currents shown at 20 μsec intervals for the time period 640–740 μsec after the initiation of the plasma current.

As expected, based on the arguments given in the Introduction, $\lambda_{\|}$ is not a constant function. Comparison of the toroidal field profiles in Fig. 2 ($y/a = 0.5$) and Fig. 6 demonstrates the result of nonconstant λ.

The location of the magnetic separatrix may be estimated by locating the positions of the poloidal magnetic field nulls. In a cylindrical approximation which assumes the

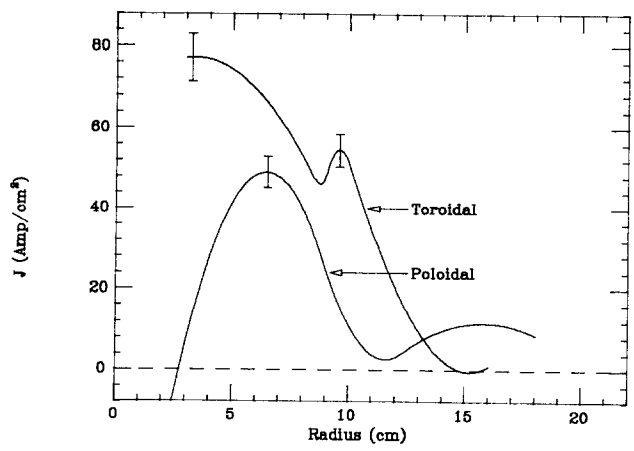

FIG. 7. The toroidal and poloidal plasma current density profiles at 680 μsec.

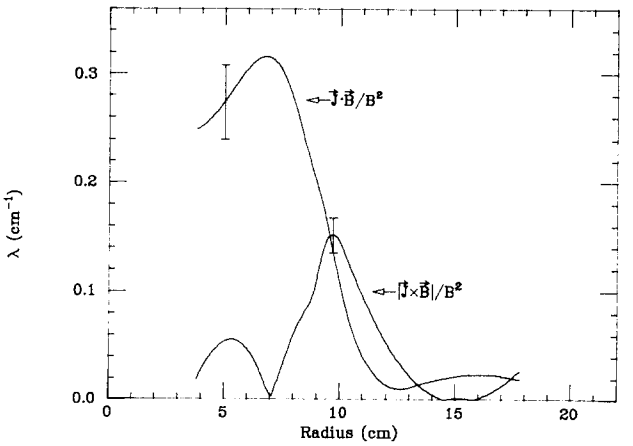

FIG. 8. The parallel ($\mathbf{J}\cdot\mathbf{B}/B^2$) and perpendicular ($|\mathbf{J}\times\mathbf{B}|/B^2$) λ profiles at 680 μsec.

plasma current is symmetrically distributed about the minor axis, these nulls lie along the diagonals of the square boundary at the points where the octupole component balances the plasma component of the poloidal magnetic field. This geometry is identical to that used to find the constant-λ magnetic equilibria described in the previous section of this paper. Assuming the plasma current I_P, flows within the radius r, the plasma contribution is simply $B_\theta^P = \mu_0 I_P/2\pi r$. By linear superposition, the ring contribution is

$$B_\theta^R = \frac{\mu_0 I_R}{2\pi d}\frac{\epsilon^3}{1-\epsilon^4}, \quad \epsilon = \frac{r}{d},$$

where d is the diagonal length from the minor axis to the center of the rings and I_R is the total ring current. By approximating the separatrix boundary as square shaped, the location where the separatrix crosses the midplane, x_{sep}, may be estimated. The advantage of this simple model is that it only requires knowledge of I_P and I_R, while providing a reasonably accurate location of the separatrix when compared with more complicated two-dimensional equilibrium calculations. For the plasmas discussed here, $B_\theta^P = B_\theta^R$ implies $x_{\text{sep}} = 10 \pm 1$ cm during the 100 μsec time period of interest.

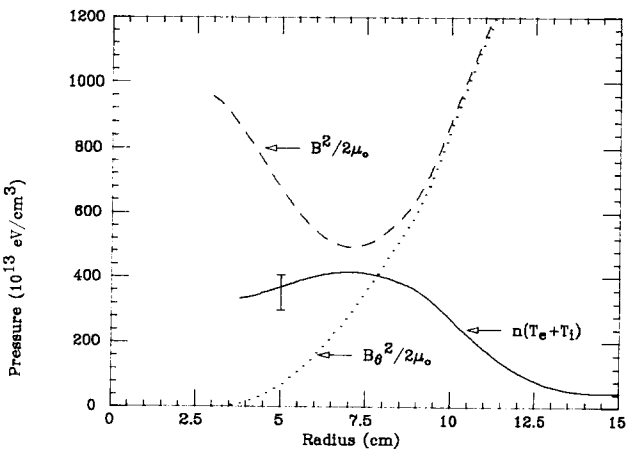

FIG. 9. The plasma pressure profile obtained from the force balance relation $\mathbf{J}\times\mathbf{B} = \nabla p$ at 680 μsec. Overlaid are the total and poloidal magnetic pressure profiles.

There are several interesting features associated with the current profiles. The first is the double peak in the poloidal current; the off-axis zero, interestingly, falls in the separatrix region. The "second" peak at $x \sim 15$ cm is a parallel current giving rise to the small peak in $\lambda_{\|}$ at the same position. This same current, located in the common flux region and driven by the reversing toroidal field, was studied in detail by others while investigating poloidal Ohmic heating of an octupole.[16] The second striking feature is the peak in the toroidal current density at $x \sim 9$ cm. This current, as can be seen by the corresponding peak in $\lambda_{\perp}$, is a large diamagnetic current. By integrating the force balance relation, $\mathbf{J} \times \mathbf{B} = \nabla p$, the plasma pressure profile may be obtained. Figure 9 shows this profile for the data represented in Figs. 7 and 8.

The sharp gradient in the pressure, resulting in the large diamagnetic current, occurs in the separatrix region. Likewise the parallel currents fall sharply in this same region. With the exception of the parallel poloidal current that flows in the common flux region, all of the interesting plasma features are associated with the plasma interior to the separatrix region. One is thus led to think of the magnetic separatrix as a limiter. By definition, it is the boundary between two types of field topology; inside the boundary the flux surfaces are the usual nested, helical structures seen in current carrying toroidal devices while outside the boundary the field is largely poloidal as in a multipole. It is reasonable, therefore, to think of this magnetic topology as the usual RFP configuration but with a magnetic limiting boundary instead of a material limiting boundary. In addition, there is no obvious nearby conductor.

The multipole field cannot be neglected, however. The plasma pressure indicated by the force balance calculation, which is consistent with independent measurements of $n_e \sim 2 \times 10^{13}$ particles/cm^3 from a central chord microwave interferometer and $T_e \sim 70$ eV from spectroscopic measurements, results in large central $\beta = 2\mu_0 p/B^2$ values; apparently the multipole field provides much of the confinement. The magnetic pressure $B^2/2\mu_0$ is shown with the plasma pressure in Fig. 9 to illustrate this effect. The pressure profile may be used to estimate the stored kinetic energy and the energy confinement time τ_E. Such a calculation gives $\tau_E \sim 20\,\mu$sec.

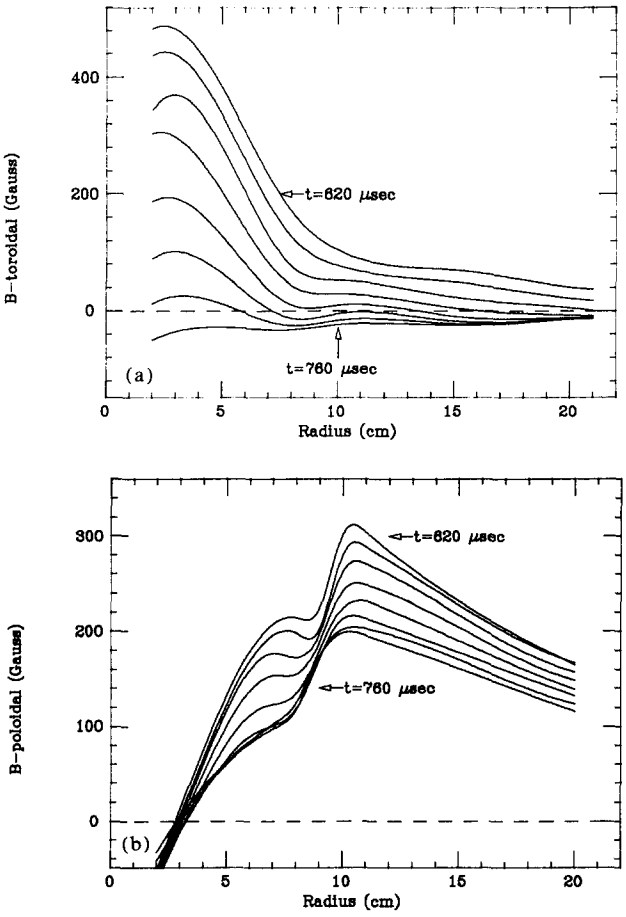

FIG. 11. Radial profiles of the (a) toroidal field and (b) poloidal field as a result of plasma currents shown at 20 μsec intervals for the time period 620–760 μsec after the initiation of the plasma current with poloidal limiters inserted.

The parallel poloidal current driven by the reversing toroidal field has the effect of slowing down the penetration of the reversal programming, i.e., this current "backwinds" the external coils. Because the plasma current is already decaying when the toroidal magnetic field reverses direction at

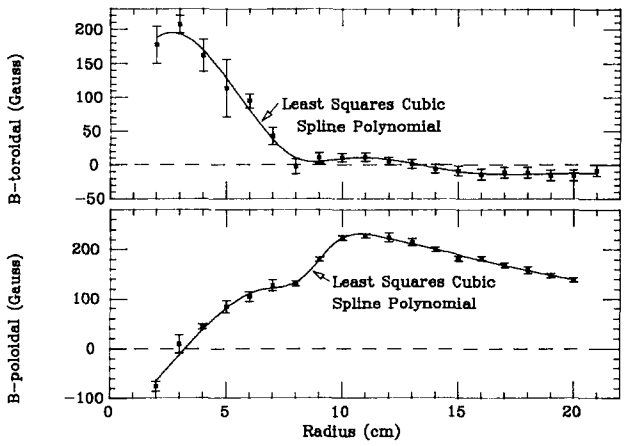

FIG. 10. Typical toroidal and poloidal (plasma component) field profile data with the poloidal limiter plates inserted. The data shown were taken at 700 μsec.

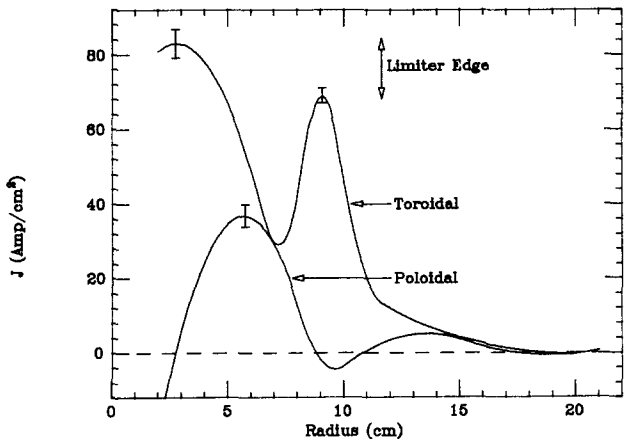

FIG. 12. The toroidal and poloidal plasma current density profiles at 700 μsec for the limited plasma.

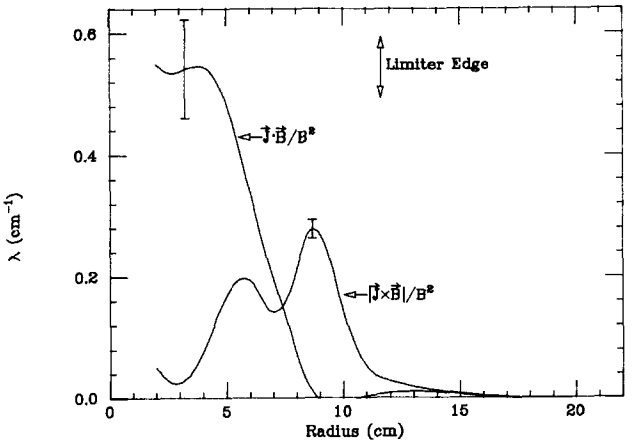

FIG. 13. The parallel and perpendicular λ profiles at 700 μsec for the limited plasma.

the wall, the additional delay resulting from this shielding effect is undesirable. To reduce this current, poloidal limiter plates were inserted into the common flux region, already magnetically limited, relying on field line helicity early in time to limit the poloidal current.

With the limiters inserted, the equilibrium profiles shown in Figs. 10 and 11 analogous to Figs. 5 and 6 were obtained. The current densities and λ profiles are likewise shown in Figs. 12 and 13. The common flux poloidal current was reduced, as desired, allowing the reversal of the toroidal field to move in more rapidly, but the reversed profile still decayed in $\sim 100\,\mu$sec. Note that the diamagnetic current is somewhat more pronounced with the poloidal limiters inserted, but the overall character of the equilibrium is similar to the unlimited case.

IV. CONCLUSIONS

This paper presented the solution of $\nabla\times\mathbf{B}=\lambda\,\mathbf{B}$, $\lambda=$ const, in a rectangular domain allowing for current sources. This solution was used to predict the flux plots and field profiles in the Tokapole II geometry. Experiments on Tokapole II, which provided the actual field, current, and λ profiles, were then described.

The expected result that $\lambda_{\|}$ is not constant was confirmed by the direct equilibrium measurements. The large currents that the constant-λ model requires in the common and private flux regions simply cannot be driven by the small parallel electric fields that are applied. However, the separatrix was found to serve as the limiting boundary for the plasma pressure and currents, and the region interior to the separatrix is described by λ profiles very similar to the RFP. In analogy to the Bessel function model, the constant-λ solution of this paper may provide a useful description of the equilibria for this region within the separatrix, since the separatrix is most nearly rectangular in shape.

Sustained reversed-field plasmas in the Tokapole II configuration were not demonstrated. As a result of hardware limitations of both the applied toroidal electric field and transformer core volt seconds, the toroidal plasma current could not be maintained ($I_P R_P \geqslant 50$ V at peak current); lack of sustainment of Tokapole II plasmas may be a result of these limitations. In order to investigate the possibility of sustainment of reversed-field plasmas in poloidal divertor configuration, these experiments are being extended to a larger (1.39 m major diameter, 1.0 m^2 cross-sectional area) device with optimized internal rings and a larger applied toroidal electric field.

ACKNOWLEDGMENTS

We are indebted to Professor R. N. Dexter, Professor D. W. Kerst, and Professor S. C. Prager for useful discussions and assistance.

This work was supported by the U. S. Department of Energy. The work of one of the authors (J. S. S.) was performed under appointment of the Magnetic Fusion Energy Technology Fellowship program which is administered for the U. S. Department of Energy by Oak Ridge Associated Universities.

[1] H. A. B. Bodin and A. A. Newton, Nucl. Fusion **20**, 1255 (1980).
[2] D. A. Baker and W. E. Quinn, in *Fusion*, edited by E. Teller (Academic, New York, 1981), Vol. 1, Part A, Chap. 7.
[3] A number of papers summarizing the present status of RFP devices are located in *Plasma Physics and Controlled Nuclear Fusion Research*, 1984, Proceedings of the 10th International Conference, London (IAEA, Vienna, 1985), Vol. 2, pp. 431–459.
[4] E. P. Butt, H. C. Cole, A. N. Dellis, A. Gibson, M. Rusbridge, and D. Wort, in *Plasma Physics and Controlled Nuclear Fusion Research*, 1965, Proceedings of the 2nd International Conference, Culham (IAEA, Vienna, 1966), Vol. 2, p. 751.
[5] T. G. Cowling, *Magnetohydrodynamics* (Hilger, Bristol, England, 1976).
[6] S. C. Prager and L. Turner, Phys. Fluids **28**, 1155 (1985).
[7] J. B. Taylor, Phys. Rev. Lett. **33**, 1139 (1974).
[8] R. Lüst and A. Schlüter, Z. Astrophys. **34**, 263 (1954); S. Chandrasekhar, Proc. Natl. Acad. Sci. U.S.A. **43**, 24 (1957); S. Chandrasekhar and P. C. Kendall, Astrophys. J. **126**, 457 (1957); S. Chandrasekhar and L. Woltjer, Proc. Natl. Acad. Sci. U.S.A. **44**, 285, 489, 833 (1958); D. R. Wells, J. Plasma Phys. **4**, 645 (1970).
[9] L. Turner, Phys. Fluids **27**, 1677 (1984).
[10] M. N. Rosenbluth and M. N. Bussac, Nucl. Fusion **19**, 489 (1979); W. C. Turner, G. C. Goldenbaum, E. H. A. Granneman, J. H. Hammer, C. W. Hartman, D. S. Prono, and J. Taska, Phys. Fluids **26**, 1965 (1983).
[11] R. J. La Haye, T. H. Jensen, P. S. C. Lee, R. W. Moore, and T. Ohkawa, Nucl. Fusion **26**, 255 (1986).
[12] A. P. Biddle, R. N. Dexter, R. J. Groebner, D. J. Holly, B. Lipschultz, M. W. Phillips, S. C. Prager, and J. C. Sprott, Nucl. Fusion **19**, 1509 (1979).
[13] K. F. Schoenberg, R. F. Gribble, and J. A. Phillips, Nucl. Fusion **22**, 1433 (1982).
[14] V. Antoni and S. Ortolani, Plasma Phys. **25**, 799 (1983).
[15] R. J. La Haye, T. N. Carlstrom, R. R. Goforth, G. L. Jackson, M. J. Schaffer, T. Tamano, and P. L. Taylor, Phys. Fluids **27**, 2576 (1984).
[16] D. J. Holly, S. C. Prager, and J. C. Sprott, Phys. Fluids **26**, 3435 (1983).